Radio-frequency transistors from millimeter-scale graphene domains*

Wei Zi-Jun(魏子钧)[a], Fu Yun-Yi(傅云义)[a]†, Liu Jing-Bo(刘竞博)[b], Wang Zi-Dong(王紫东)[a], Jia Yue-Hui(贾越辉)[a,c], Guo Jian(郭 剑)[a], Ren Li-Ming(任黎明)[a], Chen Yuan-Fu(陈远富)[b], Zhang Han(张 酣)[c], Huang Ru(黄 如)[a], and Zhang Xing(张 兴)[a]

[a] *Institute of Microelectronics, Peking University, Beijing* 100871, *China*

[b] *State Key Laboratory of Electronic Thin Films and Integrated Devices, University of Electronic Science and Technology of China, Chengdu* 610054, *China*

[c] *School of Physics, Peking University, Beijing* 100871, *China*

(Received 25 March 2014; revised manuscript received 5 May 2014; published online 24 September 2014)

Graphene is a new promising candidate for application in radio-frequency (RF) electronics due to its excellent electronic properties such as ultrahigh carrier mobility, large threshold current density, and high saturation velocity. Recently, much progress has been made in the graphene-based RF field-effect transistors (RF-FETs). Here we present for the first time the high-performance top-gated RF transistors using millimeter-scale single graphene domain on a SiO_2/Si substrate through a conventional microfabrication process. A maximum cut-off frequency of 178 GHz and a peak maximum oscillation frequency of 35 GHz are achieved in the graphene-domain-based FET with a gate length of 50 nm and 150 nm, respectively. This work shows that the millimeter-scale single graphene domain has great potential applications in RF devices and circuits.

Keywords: millimeter-scale graphene domain, radio-frequency transistor, cut-off frequency, maximum oscillation frequency

PACS: 72.20.Fr, 72.80.Vp, 87.50.S– **DOI:** 10.1088/1674-1056/23/11/117201

1. Introduction

Graphene, one-atom-thick film of carbon, comes into being as a highly promising candidate for application in radio-frequency (RF) devices due to its excellent electronic properties, such as an ultrahigh carrier mobility (2×10^5 cm^2/V·s),[1] a large threshold current density (2×10^8 A/cm^2),[2] and a high saturation velocity ($\sim5.5\times10^7$ cm/s).[3] In recent years, much progress has been made in the synthesis of graphene.[4–7] Large-area, even wafer-scale, graphene has been readily prepared by the thermal decomposition of SiC[4] or chemical vapor deposition (CVD) method.[5–7] The significant advances in graphene synthesis provide practical opportunities for developing graphene-based RF transistors. In 2010, scientists at IBM demonstrated 100-GHz transistors using wafer-scale epitaxial graphene.[8] Since then, the performance of graphene RF devices has been greatly improved. The values of cut-off frequency (f_T) of graphene transistors have reached up to 300 GHz, 350 GHz,[9] and 427 GHz[10] using epitaxial, CVD and mechanically exfoliated graphene, respectively. The maximum oscillation frequency (f_{max}) of the RF transistor has achieved 70 GHz using epitaxial graphene on SiC.[11] The above significant improvements in RF performances mainly result from continuous efforts to make high-quality graphene, to utilize a new substrate (e.g., a diamond-like carbon film, DLC),[12] and to develop the fabrication process (e.g., a self-aligned process).[10,13] The ultimate performance of the graphene-based RF transistors as indicated in Ref. [10], is primarily limited by the quality of graphene. Hence, it is highly desirable to grow high-quality graphene with a lower defect density for RF application. Recently, the process of growing large-domain single crystalline graphene has been successfully developed.[14–16] The lateral size of an individual graphene domain can range from several micrometers to 1 centimeter.[15,16] Generally, there is no grain boundary within a large-domain single-crystal graphene, which can eliminate carriers scattering from the grain boundary to possess excellent electronic properties, such as a carrier mobility as high as 1.6×10^4 cm$^2\cdot$V$^{-1}\cdot$s^{-1}.[14] It is worth noting that all the channel materials used in reported RF-FETs so far are polycrystalline graphenes. No studies have yet been performed to evaluate the performance of RF transistors made from an individual domain or single-crystal graphene. In this paper, we explore the feasibility of developing high-performance field-effect transistors (RF-FETs) using the millimeter-scale single graphene domain. The cut-off frequency (f_T) and maximum oscillation frequency (f_{max}) of this kind of RF transistor can achieve as high as 178 GHz and 35 GHz, respectively.

*Project supported by the National Basic Research Program of China (Grant Nos. 2011CBA00600, 2011CBA00601, and 2013CBA01604), the National Natural Science Foundation of China (Grant No. 60625403), and the National Science and Technology Major Project of China (Grant No. 2011ZX02707).

†Corresponding author. E-mail: yyfu@pku.edu.cn

© 2014 Chinese Physical Society and IOP Publishing Ltd

2. Experiment

Graphene with a large domain size was grown by the chemical vapor deposition (CVD) method, as reported by Zhou *et al.*[14] The copper foil was first loaded into the CVD system with a 4-inch quartz tube, which was pumped down to 5×10^{-4} Pa and refilled with 100 sccm of ultra-pure Ar gas (99.999%). The sample was then heated to 1070 °C within 40 min followed by a 5 min stabilization period with a pressure of 1700 Pa. The 50 sccm of diluted methane (1000 p.p.m. balanced in argon) and 50 sccm of hydrogen (99.999%) were introduced into the CVD system for the graphene growth at 1070 °C for 8 h under a pressure of 7.6×10^4 Pa. The growth was terminated by rapidly cooling the quartz tube to room temperature at a rate of 100 °C/min. After growth, the graphene was transferred onto the high-resistivity Si substrate (> 20 kΩ·cm) covered with a 300-nm-thick thermally grown SiO_2.

The transfer process was made using a temporary PMMA film. One side of the graphene/Cu foils was first spin-coated by polymethylmethacrylate (PMMA) and subsequently sacrificially etched in a solution of $FeCl_3$ for 12 h. The free-standing PMMA/graphene membrane was transferred from the etchant bath to the DI water. The PMMA-protected graphene was floated on the solution of $HCl/H_2O_2/H_2O$ (1:1:20) for 15 min to remove the residual impurities, followed by washing in the DI water again to remove the residual HCl. To further remove the residual organic impurities, the PMMA/graphene membrane was floated on the $NH_4OH/H_2O_2/H_2O$ (1:1:20) solution for 15 min followed by dipping it in the DI water to remove the residual NH_4OH.[17] The PMMA/graphene was transferred onto the target substrate and cured at 150 °C for 10 min after natural drying. The PMMA was removed using acetone and alcohol for 2 h respectively, and the graphene was finally transferred onto the surface of a highly resistive Si/SiO_2 substrate. The Raman spectra of the graphene were collected by a micro-Raman spectrometer with an excitation energy of 1.96 eV (633 nm).

A top-gated, dual-channel graphene RF-FET was fabricated by a CMOS-compatible top–down process. The graphene channel was patterned using e-beam lithography (EBL) followed by induced coupled plasma reactive ion etching (ICP-RIE). The source (S), drain (D), and gate (G) electrodes were defined by EBL lithography, e-beam metal evaporation and a lift-off process. The metal of S/D contacts was Pd/Au (20 nm/40 nm), which was expected to enable low contact resistance;[18] the gate electrode is a 70-nm-thick Au layer. The gate dielectric, a layer of 10-nm Al_2O_3, was grown by atom layer deposition (ALD). To deposit a conformal dielectric layer, a thin layer of Al (∼2 nm thick) was pre-deposited on the graphene surface by e-beam evaporation, which was then naturally oxidized as the ALD seeds. It was found that this ALD process of dielectrics can greatly improve the interface between graphene and the Al_2O_3, which can better maintain the intrinsic electronic properties of graphene.[19,20] The structure of RF-FETs was inspected by an optical microscope (Olympus, BX 51) and a field-emission scanning electron microscope (FE-SEM, FEI NanoSEM 430). The radio-frequency (RF) and direct current (DC) measurements were carried out on a probe station (Cascade Summit 11101B) using HP 4156C precision semiconductor parameter analyzer and Agilent E8363B network analyzer. Both DC and RF characteristics of graphene transistors were obtained at room temperature under ambient conditions.

3. Results and discussion

The RF-FETs are fabricated based on single-domain monolayer graphene thin films. Figure 1(a) shows a representative hexagon-shaped graphene domain with a size up to ∼2 mm. The corresponding Raman spectra measured at the various positions in this graphene domain are shown in Fig. 1(b). There are two peaks in each of these Raman spectra, i.e., the G peak at 1591–1593 cm^{-1} and the 2D peak at 2643–2645 cm^{-1}. The symmetric 2D peak in each of the Raman spectra can be well fitted by a single, Lorentzian function. The single 2D peaks with full width at half maximum (FWHM) values of 35–39 cm^{-1} and the peak intensity ratio $I_{2D}/I_G > 1$

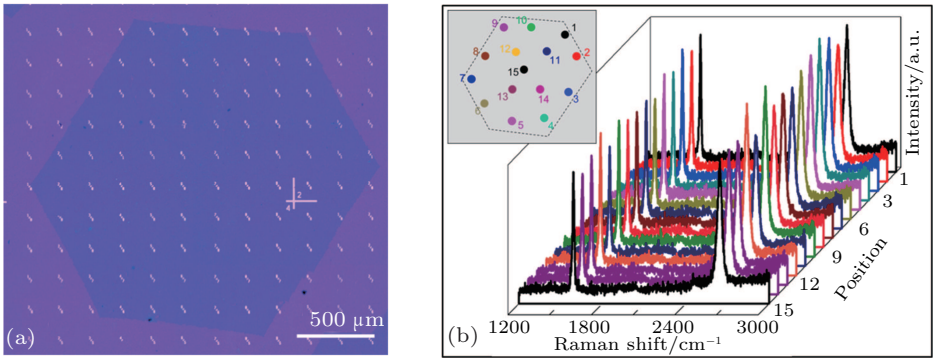


Fig. 1. (color online) A millimeter-scale graphene domain. (a) Low-magnification optical image showing an individual hexagonal graphene domain; and the micro-scale patterns on the SiO_2/Si substrate are the Ti/Au markers for microfabrication; (b) the corresponding Raman spectra in the ranges marked by numbers. The hexagon in the inset is a schematic drawing of a graphene domain in panel (a).

suggests that this domain is a monolayer graphene.[5,21] It is noted that no discernible Raman D-peak (disorder-induced general at ~1345 cm^{-1}) is observed, which indicates that the graphene domain is a high-quality crystal without defects (or defects are almost undetectable).[21] The uniformity of the millimeter-scale graphene domain is much better than that of the polycrystalline CVD graphene since the spectral features of the Raman spectra taken from different positions on this graphene domain are nearly the same (see Fig. 1(b)).

Dual-channel graphene RF transistors with a ground–signal–ground (G–S–G) configuration are fabricated by a top–down process. Figure 2(a) shows the schematic illustration of the graphene RF transistor on the SiO_2/Si substrate. A low-magnification optical image of arrays of the RF transistors using a single graphene domain is shown in Fig. 2(b). Figure 2(c) shows the SEM image of a graphene RF transistor with two gate fingers. An enlarged SEM image of a graphene RF-FET with a 50-nm gate length is shown in Fig. 2(d). The top gate is well aligned with the source/drain electrodes. The un-gated region between gate and source/drain is only about 20 nm, which can reduce the serial access resistance.

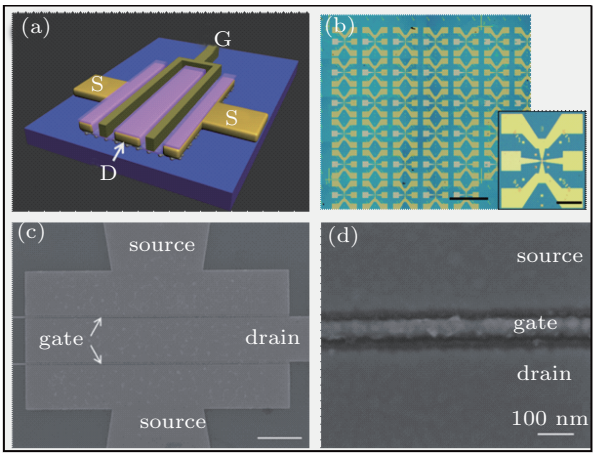


Fig. 2. (color online) Schematic, optical and SEM images of graphene RF transistors. (a) Schematic diagram of a top-gated, dual-channel graphene RF transistor on the high-resistivity Si/SiO_2 substrate. (b) Optical image of RF transistor arrays, scale bar being 500 μm. (Inset) optical image of an RF transistor with a G-S-G configuration, scale bar being 500 μm. (c) SEM image of a typical top-gated dual-channel RF device. (d) An enlarged SEM image of a graphene RF transistor with a gate length of 50 nm.

Figure 3 shows the typical transfer and output characteristics for graphene transistors with various gate lengths. The drain current (I_{DS}) of the graphene transistors shows n-type FET characteristics since the Dirac point (the minimum drain current) is always observed at $V_G < 0$ V. A similar doping behavior is also previously observed in graphene FETs fabricated on SiC[8] and DLC[12] substrates. Generally, the back-gated graphene transistors fabricated on SiO_2/Si exposed to ambient environment display strong p-doping.[22] For our top-gated graphene FETs, the exact reason for n-doping remains unclear but may be due to the doping effect from the top-gate dielectric (Al_2O_3) deposition.[9] With the gate length scaling down both the Dirac point voltage (V_{DP}) and the on/off ratio of the graphene FETs will change. The V_{DP} will exhibit a negative shift (e.g., from −1.8 V to −3.8 V) and the on/off ratio will decrease from ~4.8 to ~1.7 when the gate length is scaled from 1 μm down to 50 nm as shown in Figs. 3(a)–3(c). The variation of V_{DP} and the decrease of on/off ratio are mainly attributed to two reasons: one is the short-channel effect, which is ascribed to low electrostatic influence efficiency on the graphene channel; the other is the contact resistance, whose influence may become more pronounced in short channel graphene transistors.

The contact resistance (R_C) can be estimated from the saturated resistance ($R_{residual}$) at high top-gate voltage.[23] As shown in Figs. 3(a)–3(c), the values of drain current (I_{SD}) in the graphene transistors with various gate lengths all exhibit a tendency to saturate as the gate voltage (V_G) increases more positively. At a saturated point of I_{DS} (e.g., $V_G = 5$ V), the total device resistance can be considered to be nearly equal to the saturated resistance ($R_{residual}$) due to the fact that the resistance of heavily doped graphene in the short-channel case can be neglected.[23,24] The $R_{residual}$ is thus equal to $2R_C$. Hence, the contact resistance R_C is estimated to be in the range of 238 Ω·μm–263 Ω·μm from the transfer characteristics of five 50-nm-gate graphene transistors. These R_C values are much lower than the theoretical value (403 Ω·μm) for single-sided Pd contact, which is calculated by using density-functional theory and non-equilibrium Green's function methods.[25] The low contact resistance in our graphene transistor is mainly attributed to both the Pd/Au electrodes and the high quality of graphene. The millimeter-scale graphene domain is a high-quality crystal with no detectable defects as shown in Raman spectra (Fig. 1(b)). The Pd/Au contact is expected to exhibit relatively low contact resistance compared with other noble metals, such as titanium.[26]

The field effect mobility μ_{FE} of graphene can be approximated as

$$\mu_{FE} = \frac{g_m L^2}{C_G V_{DS}}, \tag{1}$$

where g_m is the transconductance, L is the gate length, C_G is the gate capacitance, and V_{DS} is the drain voltage. C_G consists of gate–drain capacitance (C_{GD}) and gate–source capacitance (C_{GS}), which can be extracted from the high-frequency S-parameter measurements. The estimated electron mobility is 1504 cm^2/Vs for the specified 1-μm-gate transistor (see Fig. 3(c)), corresponding to the electron concentration of ~ 1.65×10^{12} cm^2 at room temperature. The as-estimated electron mobility ranges from 1411 cm^2/Vs to 1564 cm^2/Vs for the 1-μm-gate transistors in our research.

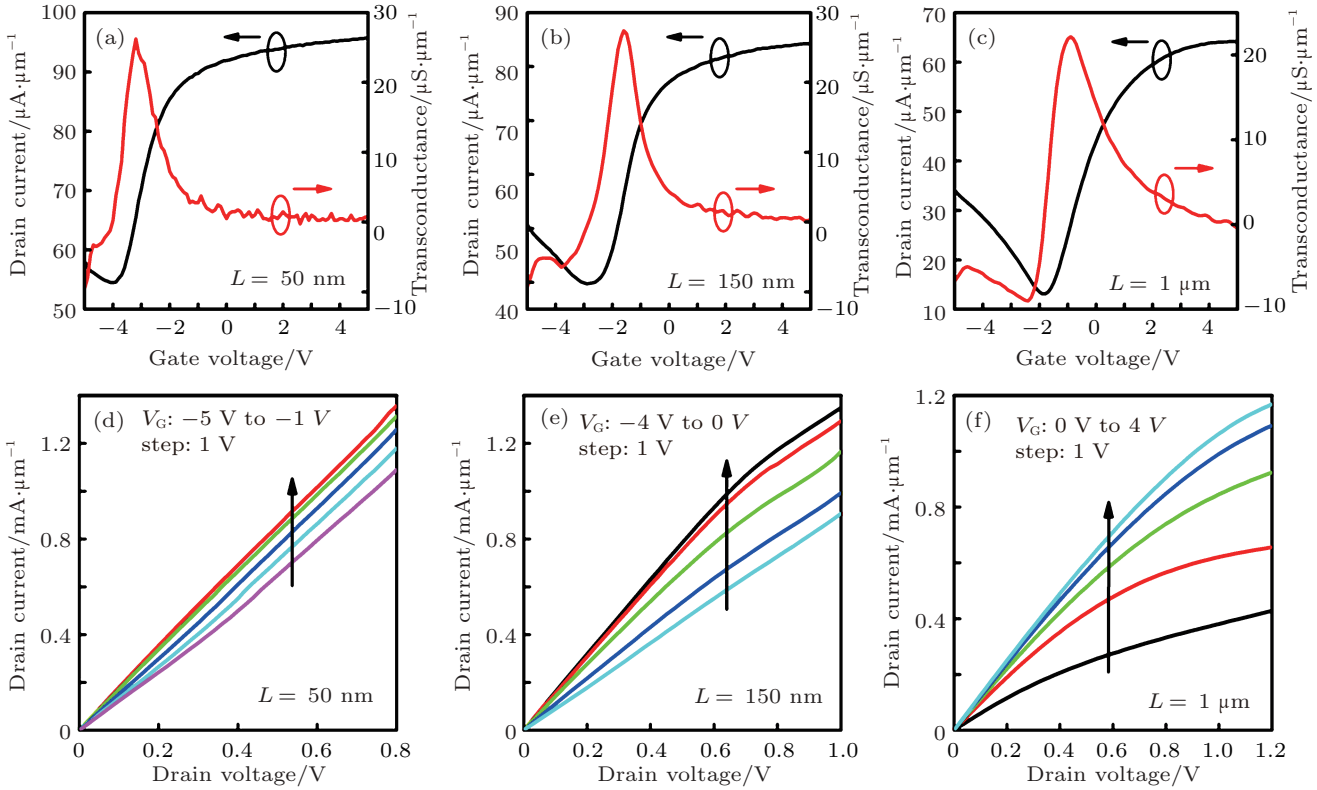


Fig. 3. (color online) Transfer and output characteristics for graphene RF transistors with gate lengths of (a, d) 50 nm, (b, e) 150 nm and (c, f) 1 μm, respectively. Transfer characteristics are measured at drain-source voltage V_{DS} of 50 mV. Curves of transconductance g_m versus gate voltage are shown in panels (a)–(c) (right y axis).

According to the model proposed in Ref. [27], the electrical transport in the graphene transistor exhibits a transition from diffusion transport to ballistic transport with the decrease of gate length. The estimated mean free path (MFP) of our graphene domain is roughly in the range of 300 nm–600 nm, which is much larger than that of polycrystalline graphene (50 nm–110 nm).[28]

The RF performances of graphene transistors are characterized by measuring S parameters in a frequency range from 100 MHz to 30 GHz by an Agilent E8363B network analyzer. A ground–signal–ground (G–S–G) configuration is adopted for the RF measurements. A careful open-short de-embedding procedure is used to remove the parasitic capacitances and resistances and evaluate the intrinsic RF performances of the graphene transistors.[8–13] The on-chip "open" and "short" structures are fabricated with exactly the same layout as that in the graphene transistor, in which no graphene exists in the "open" structure nor the gate, while the source and drain are shortened by Pd/Au metal in the "short" structure.

The cut-off frequency (f_T) is a key figure of merit for the RF circuit design, at which frequency, the short-circuit small-signal current gain $|h_{21}|$ of a graphene transistor drops to unity. The f_T is theoretically predicted to be proportional to g_m/C_G. The DC characteristics of the graphene transistors thus provide a reference for selecting an appropriate DC bias. In RF measurements, the electron conduction branch, with higher transconductance, is chosen to evaluate f_T of the graphene transistor. Figure 4(a) displays the values of intrinsic current gain $|h_{21}|$ of the three graphene transistors with gate lengths of 1 μm, 600 nm, and 150 nm, showing cut-off frequencies of 20 GHz, 34 GHz, and 85 GHz, respectively, by an ideal −20 dB/dec linear extrapolation. The cut-off frequency reaches 178 GHz after the de-embedding when scaling the gate length down to 50 nm. The Gummel's method is employed to verify the accuracy of the cut-off frequency obtained by linear extrapolation.[9,10] The consistency between the two methods confirms the accuracy of the f_T value, as shown in the inset of Fig. 4(b).

Figure 4(c) shows the gate length dependences of the cut-off frequency. The top five highest cut-off frequencies for each gate length are counted and plotted. The dependence of the f_T curve exhibits a $1/L$ trend, which is in good agreement with that in previous reports.[9,12] The f_T variations for graphene transistors of the same gate size, especially in the channel case ($L \leq 300$ nm), may result from the variation of the channel mobility.[8] From this f_T–L curve, the further scaling down of the gate length is still an effective way to reach a much higher f_T. Note that the dependence of f_T does not follow a theoretically predicted $1/L^2$ relation, which suggests that the contact resistance (R_C) may limit the device performances in the short-channel graphene transistors.[12]

Another important RF characteristic is the maximum oscillation frequency f_{max}, defined as the frequency at which the power gain of the graphene transistor falls to unity. The

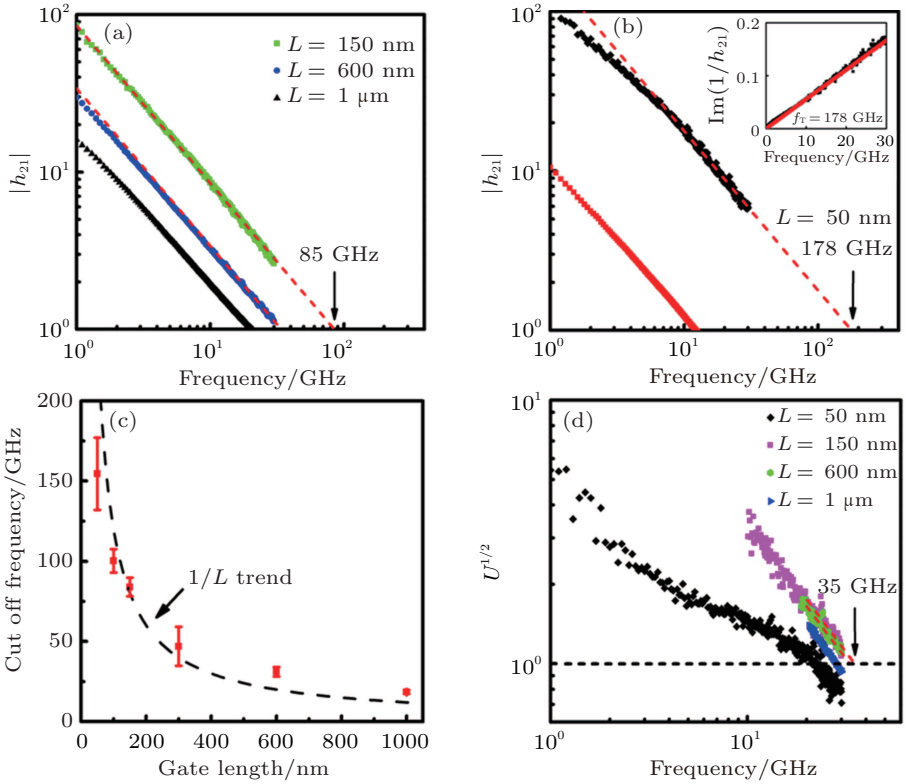


Fig. 4. (color online) Radio-frequency performances of FETs using millimeter-scale graphene domains. (a) Variations of de-embedded small-signal current gain $|h_{21}|$ with frequency for a 150-nm-gate (■), a 600-nm-gate (●), and a 1-μm-gate (▲) graphene FET. The cut-off frequencies are 85 GHz, 34 GHz, and 20 GHz for the 150-nm, 600-nm, and 1-μm devices, respectively. (b) Curves of small-signal current gain $|h_{21}|$ versus frequency for a 50-nm-gate graphene FET before (■) and after (♦) de-embedding. The inset shows the linear fitting using Gummel's method. (c) Variations of peak f_T with gate length (L), obtained from 30 devices; the dashed line denotes a $1/L$ dependence; and (d) Mason's unilateral power gains versus frequency for the four devices. A peak f_{max} of 35 GHz is obtained from the 150-nm device.

Mason unilateral power gain U is extracted from the de-embedded S parameters and plotted in Fig. 4(d). Here, U is introduced only when the transistor acts as an amplifier with unconditional stability (i.e., stability factor $K > 1$). The maximum oscillation frequency f_{max} of 22 GHz, 33 GHz, and 29 GHz are obtained for the transistors with the gate lengths of 50 nm, 600 nm, and 1 μm, respectively. The maximum f_{max} reaches 35 GHz for the transistor with $L = 150$ nm. The available f_{max} further confirms the accuracy of our de-embedding process. Unlike the gate length dependence trend of f_T, f_{max} does not increase continuously, but exhibits a peak value when scaling down the gate length of RF transistors.[9,10] The f_{max}, representing the extrinsic performance of the device, is affected by various factors, such as output resistance (r_0), gate resistance (R_G), gate capacitor (C_G), and f_T, which lead to the nonmonotonic trend of the f_{max}–L curve and the performance gap between f_{max} and f_T.[9,12] The gate length dependence trends of f_{max} in our devices are coincident with those reported in Refs. [9] and [10]. Although the device structure is not yet fully optimized, a high cutoff frequency up to 178 GHz is realized directly on the bare SiO_2/Si substrate using a conventional microfabrication process, which demonstrates that the millimeter-scale graphene domain has great potential applications in the radio frequency technique.

4. Conclusion

In this paper, we propose a new route to develop high-performance transistors for radio-frequency (RF) applications using a single graphene domain. We successfully prepare the monolayer graphene domain with a size up to ~2 mm. No discernible Raman D peak is observed in the graphene domain, which indicates that the graphene domain is a high-quality thin film without detectable defects. Top-gated, dual-channel graphene RF transistors, each with a ground–signal–ground (G–S–G) configuration, are fabricated by a CMOS compatible top–down process on the high-resistivity Si/SiO_2 substrates. Three graphene transistors with gate lengths of 1 μm, 600 nm, and 150 nm are achieved to have cut-off frequencies of 20 GHz, 34 GHz, and 85 GHz, respectively. The cut-off frequency reaches up to 178 GHz when scaling the gate length down to 50 nm. A maximum oscillation frequency f_{max} of the 150-nm transistor reaches 35 GHz. Our work demonstrates that it is feasible to create high-performance RF-FETs using the millimeter-scale single graphene domain, which will have great potential applications in radio-frequency electronics. Most recently, the wafer-scale growth of single-crystal graphene has been demonstrated on the surface of hydrogen-terminated Ge (110) or Ge (111).[29] It is suggested that our work may open up possibilities of achieving the wafer-scale

RF integrated circuit using single-crystal graphene.

Acknowledgment

The authors thank Y. Q. Wu, J. C. Wen, L. Ye, Y. Wu, and J. J. Zhou for insightful discussion, and W. G. Chu, F. L. Dong, B. Q. Chen, and H. Y. Lu for expert technical support. We are grateful to J. C. Wen, W. Zhu, Z. J. Zhou, and X. J. Shu in HDU for technique support of high-frequency measurements.

References

[1] Bolotin K I, Sikes K J, Jiang Z, Klima M, Fudenberg G, Hone J, Kim P and Stormer H L 2008 *Solid State Commun.* **146** 351

[2] Novoselov K S A, Geim A K, Morozov S, Jiang D, Katsnelson M, Grigorieva I, Dubonos S V and Firsov A A 2005 *Nature* **438** 197

[3] Meric I, Han M Y, Young A F, Ozyilmaz B, Kim P and Shepard K L 2008 *Nat. Nanotech.* **3** 654

[4] Emtsev K V, Bostwick A, Horn K, Jobst J, Kellogg G L, Ley L, Jessica L M, Taisuke O, Sergey A R, Jonas R, Eli R, Andreas K S, Daniel W, Heiko B W and Thomas S 2009 *Nat. Mater.* **8** 203

[5] Li X, Cai W, An J, Kim S, Nah J, Yang D, Piner R, Velamakanni A, Jung I, Tutuc E, Banerjee S K, Colombo L and Ruoff R S 2009 *Science* **324** 1312

[6] Kim K S, Zhao Y, Jang H, Lee S Y, Kim J M, Kim K S, Ahn J H, Kim P, Choi J Y and Hong B H 2009 *Nature* **457** 706

[7] Bae S, Kim H, Lee Y, Xu X, Park J S, Zheng Y, Balakrishnan Y, Lei T, Kim H R, Song Y, Kim Y J, Kim K S, Ozyilmaz B, Ahn J H, Hong B H and Iijima S 2010 *Nat. Nanotech.* **5** 574

[8] Lin Y M, Dimitrakopoulos C, Jenkins K A, Farmer D B, Chiu H Y, Grill A and Avouris P 2010 *Science* **327** 662

[9] Wu Y Q, Jenkins K A, Valdes-Garcia A, Farmer D B, Zhu Y, Bol A A, Dimitrakopoulos C, Zhu W J, Xia F N, Avouris P and Lin Y M 2012 *Nano Lett.* **12** 3062

[10] Cheng R, Bai J W, Liao L, Zhou H L, Chen Y, Liu L X, Lin Y C, Jiang S, Huang Y and Duan X F 2012 *Proc. Nation Acad. Sci.* **109** 11588

[11] Guo Z L, Dong R, Chakraborty P S, Lourenco N, Palmer J, Hu Y K, Ruan M, Hankinson J, Kunc J, Cressler J D, Berger C and De Heer W A 2013 *Nano Lett.* **13** 942

[12] Wu Y Q, Lin Y M, Bol A A, Jenkins K A, Xia F N, Farmer D B, Zhu Y and Avouris P 2011 *Nature* **472** 74

[13] Liao L, Lin Y C, Bao M Q, Cheng R, Bai J W, Liu Y, Qu Y Q, Wang K L, Huang Y and Duan X F 2010 *Nature* **467** 305

[14] Zhou H L, Yu W J, Liu L X, Cheng R, Chen Y, Huang X Q, Liu Y, Wang Y, Huang Y and Duan X F 2013 *Nat. Commun.* **4** 2096

[15] Luo B, Liu H T, Jiang L L, Jiang L, Geng D C, Wu B, Hu W Q, Liu Y Q and Yu G 2013 *J. Mater. Chem. C* **1** 2990

[16] Hao Y F, Bharathi M S, Wang L, Liu Y Y, Chen H, Nie S, Wang X H, Chou H, Tan C, Fallahazad B, Ramanarayan H, Magnuson C W, Tutuc E, Yakobson B I, McCarty K F, Zhang Y W, Kim P, Hone J, Colombo L and Ruoffl R S 2013 *Science* **342** 720

[17] Liang X L, Sperling B A, Calizo I, Cheng G J, Hacker C A, Zhang Q, Obeng Y, Yan K, Peng H L, Li Q L, Zhu X X, Yuan H, Hight Walker A R, Liu Z F, Peng L M and Richter C A 2011 *ACS Nano.* **5** 9144

[18] Song S M, Park J K, Sul O J and Cho B J 2012 *Nano Lett.* **12** 3887

[19] Kim S, Nah J, Jo I, Shahrjerdi D, Colombo L, Yao Z, Tutuc E and Banerjee S K 2009 *Appl. Phys. Lett.* **94** 062107

[20] Lin Y M, Jenkins K, Farmer D, Valdes-Garcia A, Avouris P, Sung C Y, Chiu H Y and Ek B 2009 *IEEE International Electron Devices Meeting (IEDM)*, December 2009 New York, USA, pp. 1–4

[21] Ferrari A C, Meyer J C, Scardaci V, Casiraghi C, Lazzeri M, Mauri F, Piscanec S, Jiang D, Novoselov K S, Roth S and Geim A K 2006 *Phys. Rev. Lett.* **97** 187401

[22] Joshi P, Romero H E, Neal A T, Toutam V K and Tadigadapa S A 2010 *J. Phys: Condens. Matter* **22** 334214

[23] Venugopal A, Colombo L and Vogel E M 2010 *Appl. Phys. Lett.* **96** 013512

[24] Liu W J, Li M F, Xu S H, Zhang Q, Zhu Y H, Pey K L, Hu H L, Shen Z X, Zou X, Wang J L, Wei J, Zhu H L and Yu H Y 2010 *IEEE International Electron Devices Meeting (IEDM)*, December 2010 San Francisco, CA, p. 23.3.1

[25] Ji X, Zhang J, Wang Y, Qian H and Yu Z 2013 *Phys. Chem. Chem. Phys.* **15** 17883

[26] Xia F N, Perebeinos V, Lin Y M, Wu Y and Avouris P 2011 *Nat. Nanotech.* **6** 179

[27] Chen Z and Appenzeller J 2008 *IEEE International Electron Devices Meeting (IEDM)*, December 2008 San Francisco, CA, pp. 1–4

[28] Chen K, Wan X, Liu D Q, Kang Z W, Xie W G, Chen J, Miao Q and Xu J B 2013 *Nanoscale* **5** 5784

[29] Lee J H, Lee E K, Joo W J, Jang Y, Kim B S, Lim J Y, Choi S H, Ahn S J, Ahn J R, Park M H, Yang C W, Choi B L, Hwang S W and Whang D 2014 *Science* **344** 2014